Phys. Status Solidi C **10**, No. 5, 794–798 (2013) / **DOI** 10.1002/pssc.201200620

physica status solidi pss c
www.pss-c.com
current topics in solid state physics

Role of bias conditions in the hot carrier degradation of AlGaN/GaN high electron mobility transistors

Shubhajit Mukherjee[*,1], Yevgeny Puzyrev[2], John Hinckley[3], Ronald D. Schrimpf[4], Daniel M. Fleetwood[2,4], Jasprit Singh[3], and Sokrates T. Pantelides[2,4]

[1] Interdisciplinary Program in Materials Science, Vanderbilt University, Nashville, TN 37212, USA
[2] Department of Physics and Astronomy, Vanderbilt University, Nashville, TN 37212, USA
[3] Department of Electrical Engineering and Computer Science, University of Michigan, Ann Arbor, MI 48109, USA
[4] Department of Electrical Engineering and Computer Science, Vanderbilt University, Nashville, TN 37212, USA

Received 26 August 2012, revised 11 January 2013, accepted 28 January 2013
Published online 27 February 2013

Keywords HEMT, AlGaN/GaN, hot carrier effects, Monte-Carlo analysis

[*] Corresponding author: e-mail shubhajit.mukherjee@vanderbilt.edu

The impacts of gate bias and device temperature on carrier energy distributions are reported for AlGaN/GaN High Electron Mobility Transistors. The lateral electric field and the average carrier energy are the highest at the end of gate on the gate-drain access side. The number of high energy carriers is the greatest in the semi-ON operating condition, with maximum energies exceeding the activation energy of defects in the AlGaN. There is a significant decrease in the number of very high energy carriers (greater than 2 eV) as the device temperature increases whereas the number of moderately energetic carriers (between 1 to 2 eV) is higher at elevated temperatures.

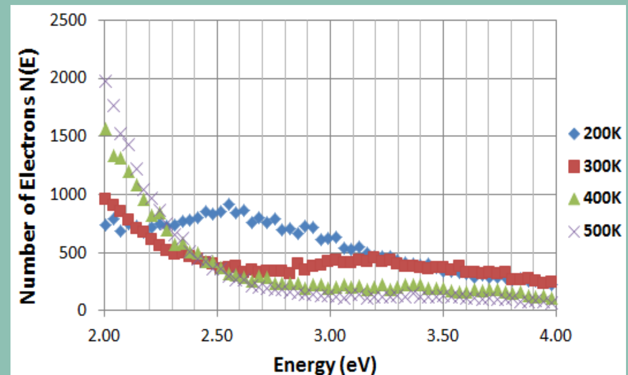

© 2013 WILEY-VCH Verlag GmbH & Co. KGaA, Weinheim

1 Introduction AlGaN/GaN high electron mobility transistors (HEMTs) have emerged as an extremely promising technology for high power and high frequency microwave applications. A combination of wide bandgap, high breakdown field and strong piezoelectric polarization effect results in high carrier mobility and large power density. Hence, GaN-based HEMTs have the best figure of merit among major power semiconductor technologies. Degradation due to hot carriers is a significant long-term reliability problem in these devices, especially in the extremely high switching speed microwave communication applications. The generation of traps by hot electrons leads to significant reduction in the drain current and transconductance, as well as large shifts in the threshold voltage. Gate lag in HEMTs is another performance issue that is affected by hot carriers [1-3].

This paper examines the impact of gate bias on the energy distribution of electrons in AlGaN/GaN HEMTs using an ensemble Monte-Carlo analysis. The percentage of high energy carriers is enhanced in the semi-ON mode of operation. A large concentration of hot carriers is generated in this state because of the presence of high field and moderate carrier density at the same time. The high-energy tail of the electron energy distribution exceeds the activation energies of several defects in AlGaN which may result in degradation. This is consistent with experiments indicating enhanced degradation in semi-ON mode [4-6]. Recent experimental work indicates that this degradation may be related to electron trapping in the gate-drain (G-D) access region induced by hot electrons [7, 8]. The effects of variation in operating temperature and device access

© 2013 WILEY-VCH Verlag GmbH & Co. KGaA, Weinheim

Contributed Article

length dimensions on the energy distribution are also reported.

2 Simulation overview

2.1 Simulator formalism The simulator used for investigating the electron energy distribution in the GaN-based HEMTs considered here is the HFET Monte-Carlo solver from Michigan. The software uses a two-dimensional Poisson and drift-diffusion solver to obtain the electric field and charge distribution along the channel. The quasi-Fermi levels obtained are used to solve the Schrodinger equation to obtain the electron wave functions and the confined energy levels. The Shockley-Read-Hall generation/recombination mechanism is included in the continuity equation. The ensemble Monte-Carlo technique is then used to simulate the electric field and the spatial velocity of electrons along the channel. This is calculated using the electric field from the steady-state mobility model. The carrier velocity is first calculated with one electron in a constant electric field. The velocity-field relationship is then obtained with 500,000 electrons in a variable electric field. Acoustic and polar optical phonon scattering are included along with alloy, equivalent/non-equivalent inter-valley, charged dislocation and interface roughness scattering effects [2].

2.2 Device description The device simulated was the AlGaN/GaN HEMT shown in Fig. 1. The AlGaN had a mole fraction of 0.32 and is 25.0 nm thick. A Schottky barrier of Φ_b = 1.68 eV is used as the gate contact. The formation of the 2DEG in an AlGaN/GaN HEMT is largely due to the simultaneous presence of spontaneous and piezoelectric polarization introduced by fixed charges. These fixed charges are represented by 1.4 × 10^{13} cm^{-2} positive charges at the AlGaN/GaN interface [3]. The GaN is 10^{15} cm^{-3} n-type, corresponding to the unintentional doping of the material. Initially, the gate, gate-source (G-S) access and gate-drain (G-D) access region, were 0.05 µm, 0.35 µm, and 1.2 µm long, respectively. The initial simulations were performed at 300 K and the threshold voltage of the device was -3.8 V. These simulations were performed with a drain bias of +10.0 V and the source contact grounded. The gate bias was varied from -9.0 V to +3.0 V, to investigate the electron energy density distributions for the ON, Semi-ON and OFF states. Additional simulations were carried out to examine the effects of the temperature and the G-S access region length variations in the semi-ON condition.

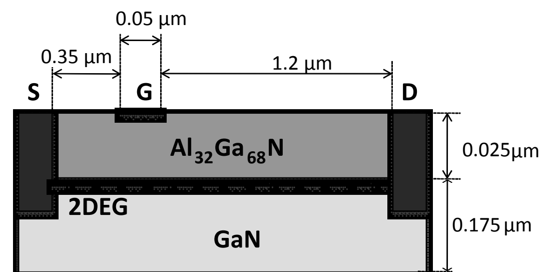

Figure 1 AlGaN/GaN HEMT device structure used for the HFET ensemble Monte-Carlo simulation.

3 Simulation results

3.1 Electric field and electron energy The longitudinal electric field becomes more positive in the G-S access region and more negative in the G-D region as V_{GS} becomes more negative, as shown in Fig. 2. The magnitude of electric field is greater in the G-D access region compared to the G-S access region. Near the end of the gate (0.4 µm), the electric field reaches its maximum magnitude in the G-D access region. When positive bias is applied to the gate, the field is slightly positive in the G-S access region and negative under the gate, although the magnitude is much lower than it is for negative gate biases. It becomes positive again in the G-D region.

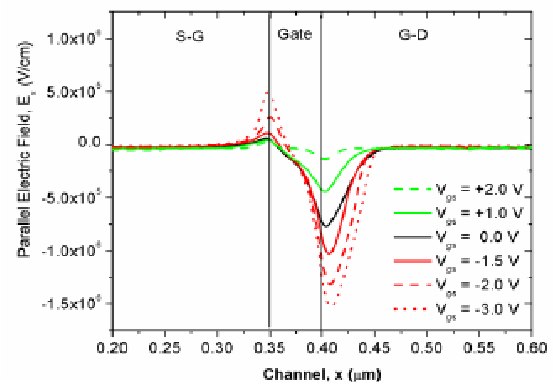

Figure 2 Lateral electric field as a function of the channel position for different gate bias with V_D = +10 V and V_S = 0 V.

The average electron kinetic energy along the channel is also strongly related to the gate bias. The electron energy is highest at the end of the gate, where the G-D access region starts. As shown in Fig. 3, this energy increases as V_{GS} becomes more negative. The energy peak falls gradually on the G-D side and abruptly on the G-S side. The energy peak gradually shifts towards the drain as V_{GS} becomes more negative. The average energy under the gate for V_{GS} = -1.5 V is nearly as large as that with V_{GS} = -3.0 V. The electron energy is low in the G-S access region.

© 2013 WILEY-VCH Verlag GmbH & Co. KGaA, Weinheim

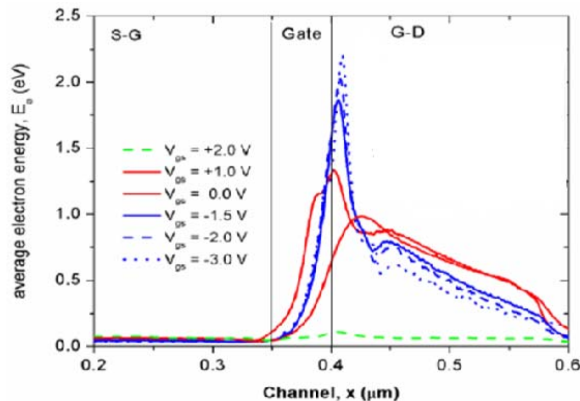

Figure 3 Average electron energy as a function of the channel position for different gate bias with V_{DS} = +10.0 V.

3.3 Electron energy distribution The number of electrons as a function of energy is shown in Fig. 4. The distribution is taken from the end of the gate on the G-D access side (at 0.4 μm), where the peaks in the average electron energy are observed for negative V_{GS}. There are peaks in energy distributions for negative V_{GS} indicating a large presence of moderately energetic (1-2 eV) electrons. The largest peaks are for the semi-ON mode, i.e., between V_{GS} = -1.5 V and V_{GS} = -2.0 V. The results are consistent with experiments indicating a substantial degradation of transconductance peak in the semi-ON state (Fig. 4 inset).

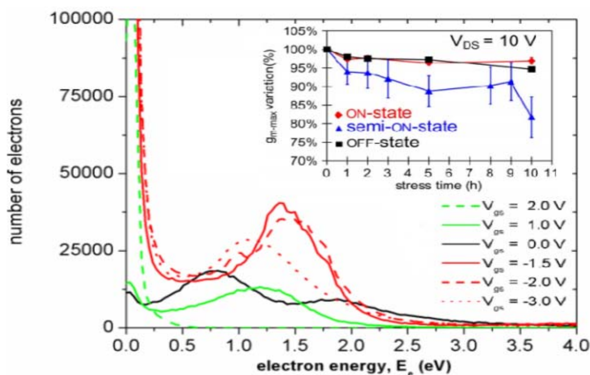

Figure 4 Electron-energy distribution with different gate-bias conditions, sliced at the end of gate on G-D side for V_{DS} = 10 V. The inset shows transconductance degradation in semi-ON [4].

The Monte-Carlo simulation results indicate that a significant percentage of electrons in the semi-ON state have energies greater than 2.5 eV, which is the activation energy for dehydrogenation of a triply hydrogenated Ga vacancy in AlGaN (H_3-V_{Ga}). The activation energies were calculated as defect migration barriers using nudged elastic band method in DFT with VASP [9, 10]. The percentage of carriers exceeding 2.5 eV in the ON and semi-ON states is reported in Table 1. The number of carriers with sufficiently high energies to form a defect like H_3-V_{Ga} in the semi-ON state was utilized to calculate the capture cross section area of the defect. The defect generation rate and the cross section area are related as following,

$$\frac{\partial}{\partial t}\Delta N_d(t) = \Sigma_{E>eact}[N_d(0) - N_d(t)]v(E)N(E)\sigma \quad (1)$$

where $N_d(t)$ is the number of activated defects at time t, E_{act} is the activation energy of H_3-V_{Ga}, $v(E)$ is the velocity of carrier with energy E, $N(E)$ is the number of carriers with energy E and σ is the capture cross-section. The defect generation rate was calculated from experimental pinch-off voltage using Eq. (2), where d_{AlGaN} is thickness of AlGaN layer. These semi-ON state stress experiments were conducted on HEMTs of similar dimensions as used in the simulations. N-rich and Ga-rich devices grown using MBE showed a positive pinch-off voltage shift with time indicating presence of H_3-V_{Ga} [11, 12].

$$\Delta V_{pinch-off}(t) = \frac{q \cdot \Delta N_d(t)}{\varepsilon} d_{AlGaN^2} \quad (2)$$

Table 1 Pinch-off voltage shift at Semi-ON, defect activation energy, high energy carrier percentage, and the capture cross section area for Ga-vacancy (H_3-V_{Ga}).

Parameters	Values
E_{act} (from DFT)	2.5 eV
$N(E>E_{act})$ (ON)	0.32 %
$N(E>E_{act})$ (semi-ON)	7.21 %
$\Delta V_{pinch-off}$(max)	0.2 V
σ (H_3-V_{Ga}, semi-ON)	1.6 x 10^{-15} cm^{-2}

The capture cross section areas of the dehydrogenated defects like H_3-V_{Ga} can be utilized to predict long-term device degradation for different gate bias and temperature conditions from accelerated stress experiments.

The presence of high density of hot carriers at the end of the gate on the gate-drain access side was qualitatively validated by hydrodynamic simulations using Sentaurus-Device TCAD from Synopsys [13]. This was done to understand the potential merits of using the HFET M-C simulator over commercial TCAD suites for III-V device simulation. The dimensions of the contacts and the access regions were exactly similar to that of the device used for the Monte-Carlo analysis. The simulations were performed at 300 K and a Schottky barrier of 1.72 eV was used to model the gate contact. A fixed charge of 1.4 × 10^{13} cm^{-2} was introduced at the AlGaN/GaN interface to represent the spontaneous and piezoelectric polarization effects. The wurtzite crystal lattice structure was considered for GaN along with the strain piezoelectric model. The simulation results show a distinct peak in the energy distribution at the end of gate on the gate-drain access side in the semi-ON condition. The carrier energy gradually decreases towards the drain. Figure 5 compares the TCAD and HFET M-C

© 2013 WILEY-VCH Verlag GmbH & Co. KGaA, Weinheim

results. The difference in the carrier energy peak for the two cases can be attributed to the 2-D multi-valley (*Γ*, *L* and *U-M* valleys) ensemble Monte-Carlo approach used to simulate the spatial velocity of electrons along the channel. The coupling of multi-valley ensemble M-C into 2-D Poisson and drift-diffusion solver results in a more accurate analysis of various scattering processes [2].

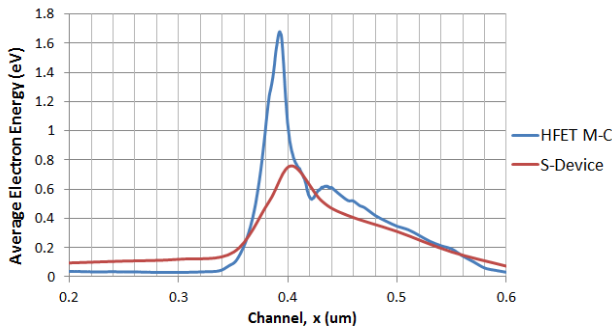

Figure 5 Carrier energy profiles along the channel in the semi-ON (V_{GS} = -1.5 V, V_{DS} = +10.0 V) condition for HFET M-C and S-Device TCAD simulations. Gate extends from 0.35 to 0.4 µm.

3.4 Effects of temperature and device geometry

The effects of device temperature variation on the electron energy distributions have also been investigated. The bias conditions were V_{GS} = -1.7 V and V_{DS} = 10 V (semi-ON), which corresponded to the maximum degradation at room temperature. The resulting electron energy distribution

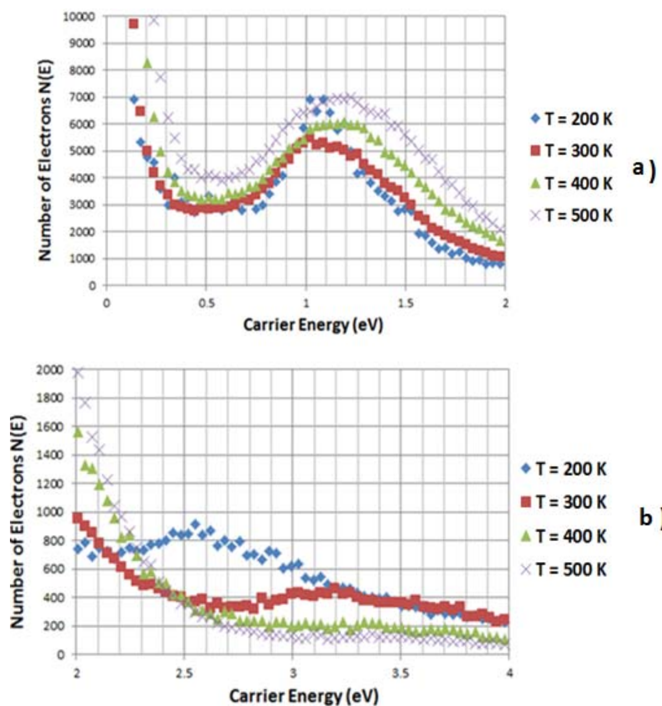

Figure 6 Energy distribution for a) intermediate energy carriers and b) high-energy (E > 2 eV) carriers at different temperatures.

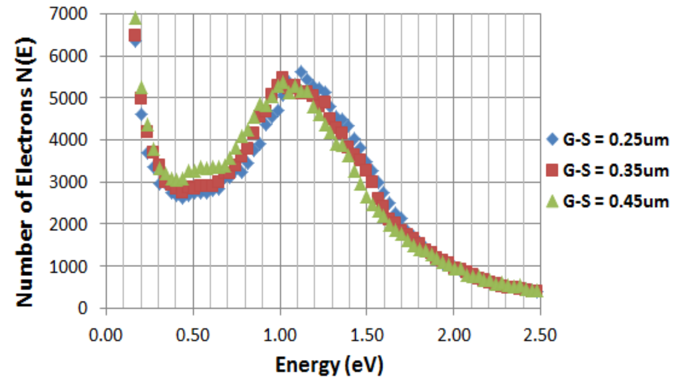

Figure 7 Electron-energy distribution profiles for the semi-ON condition (V_{GS} = -2.0 V, V_{DS} = +10.0 V) for different devices with varying gate-source access region lengths.

profiles at the end of gate on the gate-drain access region side where the carrier energy is at its highest are shown in the Figs. 6a and b.

The electron energy peaks in Fig. 6a indicate that the density of mid-energy (1 to 2 eV) carriers increases with temperature. The energy peak moves slightly higher with the increase in temperature. The high energy tails in Fig. 6b, however, show that the density of high energy carriers (E > 2 eV) is comparatively lower at higher temperatures. From Table 2, we can infer that the percentage of high energy carriers capable of causing dehydrogenation of defects in the AlGaN decreases considerably with increase in temperature. This reduction of high energy carriers can be attributed to an increase in electron-phonon interactions at the higher temperatures.

Table 2 High energy carrier distribution (for H_3-V_{Ga}) for peak semi-ON degradation condition (V_{GS} = -1.7 V, V_{DS} = +10.0 V) at different device operating temperatures.

Temperature	E > 2.5 eV
200 K	9.97 %
300 K	7.36 %
400 K	2.87 %
500 K	1.41 %

The energy distributions were then computed for devices with varying gate-source and gate-drain access lengths. There was negligible difference in the energy peaks with variation in access region lengths as can be observed from Fig. 7. The simulations were performed in the semi-ON state (V_{GS} = -2.0 V, V_{DS} = +10.0 V) at room temperature. The electron energy peak was marginally higher for the device with shorter gate-source access length due to slightly higher electric field at the end of gate on the gate-drain access side for the shorter gate-source access length devices. These results confirm that the energy distribution peak and the resulting device degradation in the semi-ON condition are largely independent of the gate-source access region length.

© 2013 WILEY-VCH Verlag GmbH & Co. KGaA, Weinheim

4 Discussion The results indicate that although the electric field and the average energy of carriers is the highest in the OFF state of operation, the total energy of carriers is at its maximum in the semi-ON state. This is due to the combined effects of high carrier energy and the relatively high density of carriers. The HFET Monte-Carlo simulations show that the carrier energy peaks near the gate in the gate-drain access region. There is a high energy tail in the semi-ON mode, when V_{GS} is in the -1.3 V to -2.5 V range with the maximum energy at V_{GS} = -1.7 V. A high percentage of these carriers have sufficient energy at room temperature to result in dehydrogenation of defects such as H_3-V_{Ga}. The density of moderately energetic carriers (between 1 to 2 eV) increases with the temperature whereas the density of very high energy carriers (E > 2 eV) decreases considerably. The results suggest that the percentage of carriers with energy high enough to dehydrogenate defects like H_3-V_{Ga} will be significantly lower at elevated temperatures for similar bias conditions. The simulations for devices with different gate-source and gate-drain access region lengths indicate that the high energy peak observed in the semi-ON state is largely independent of these factors.

References

[1] N.-Q. Zhang, S. A. Keller, G. K. Parish, S. P. DenBaars, and U. K. Mishra, IEEE Electron Device Lett. **21**, 421-424 (2000).

[2] Y.-R. Wu, M. Singh, and J. Singh, IEEE Trans. Electron Devices **53**, 588-593 (2006).

[3] C. Hodges, N. Killat, F. Gao, T. Palacios, U. K. Mishra, J. S. Speck, and M. Kuball, Appl. Phys. Lett. **100**, 112106-112109 (2012).

[4] G. Meneghesso, G. Verzellesi, F. Danesin, M. Meneghini, and E. Zanoni, IEEE Trans. Dev. Mater. Reliab. **8**, 332-343 (2008).

[5] M. Silvestri, M. J. Uren, and M. Kuball, IEEE Electron Device Lett. **33**, 1550-1552 (2012).

[6] J. Joh, F. Gao, T. Palacios, and J. A. del Alamo, Microelectron. Reliab. **50**, 767-773 (2010).

[7] M. Meneghini, N. Ronchi, A. Stocco, G. Meneghesso, U. K. Mishra, P. Yi, and E. Zanoni, IEEE Trans. Electron Devices **58**, 2996-3003 (2011).

[8] M. Meneghini, A. Stocco, R. Silvestri, A. Ronchi, G. Meneghesso, and E. Zanoni, IEEE IRPS, 2C.2.1-2C.2.5. (2012).

[9] G. Kresse and J. Furthmüller, Phys. Rev. B **54**, 11169-11186 (1996).

[10] G. Mills and H. Jonsson, Phys. Rev. Lett. **72**, 1124-1127 (1994).

[11] S. T. Pantelides, Y. Puzyrev, X. Shen, T. Roy, S. DasGupta, B. R. Tuttle, D. M. Fleetwood, and R. D. Schrimpf, Microelectron. Eng. **90**, 3-8 (2012).

[12] Y. S. Puzyrev, T. Roy, M. Beck, B. R. Tuttle, R. D. Schrimpf, D. M. Fleetwood, and S. T. Pantelides, J. Appl. Phys. **109**, 034501 (2011).

[13] Synopsys Sentaurus Device User Guide, 561-564 (2007).

© 2013 WILEY-VCH Verlag GmbH & Co. KGaA, Weinheim